Triple differential cross-section measurements for Kr($3d$) electron-impact ionization

Steven J. Cavanagh and Birgit Lohmann*
School of Science, Griffith University, Nathan, Queensland 4111, Australia
(Received 28 October 1997)

Triple differential cross sections have been measured for the electron-impact ionization of the $3d$ orbital of krypton. The measurements have been performed in asymmetric coplanar geometry at incident energies around 1 keV, and ejected electron energies of 72 eV (corresponding to bound Bethe ridge conditions) and 50 eV. Both of these energies are significantly below the binding energy of the $3d$ orbital of approximately 94 eV. The measured cross sections are compared with calculations performed in the distorted-wave Born approximation and the distorted-wave impulse approximation. There is quite good agreement in the former case, but no agreement in the latter, despite kinematics which should emphasize the impulsive nature of the collision. [S1050-2947(98)09204-X]

PACS number(s): 34.80.Dp

INTRODUCTION

Ionization of atoms by electron impact is a process which plays an important role in atomic physics, having applications in diverse areas such as astrophysics, plasma and radiation physics, and surface science. Advances in experimental techniques have meant that it is now possible to measure multiply differential cross sections for ionization, thereby offering new challenges to theories describing the process. Detailed information on the dynamics of the ionization process and the correlated behavior of the outgoing particles can be obtained via the $(e,2e)$ technique, in which the momenta of the incident, scattered, and ejected electrons are fully determined. The relationship between the momenta of the three electrons may be specified by a number of different kinematical arrangements, with different conditions emphasizing different aspects of the collision. Structure information is obtained via electron momentum spectroscopy, where the two outgoing electrons are detected with fixed polar angles of 45° relative to the incident beam direction and varying azimuthal angle (see Ref. [1] for a review). Detailed information about the collision dynamics and ionization mechanism may be obtained using the following kinematics. In the asymmetric coplanar geometry, all three electrons are detected in the same plane, and the two outgoing detected electrons have different energies and angles of emission. The fast outgoing electron is identified as the scattered electron, with momentum $\mathbf{k}_a$. The slow (ejected) electron has momentum $\mathbf{k}_b$, while the incident electron has momentum $\mathbf{k}_0$. The coplanar symmetric geometry refers to the case where the two outgoing detected electrons have equal angles (on opposite sides of the incident beam) and equal energies. A variation of the latter is the fixed relative angle geometry, in which the mutual angle between the two outgoing electrons remains constant, while the detection angle of one is varied. Geometries in which the incident momentum vector does not lie in the plane containing $\mathbf{k}_a$, and $\mathbf{k}_b$ (out-of-plane geometries) have also been employed.

Valence-shell ionization of atoms has been extensively explored using the $(e,2e)$ technique (see Ref. [2] and references therein). The results demonstrate several trends which generally typify the behavior of the measured cross section, called the triple differential cross section (TDCS). Certain kinematical arrangements enhance collisions in which the primary interaction is between the projectile and target electron, resulting in a single binary collision. For collisions in which interactions with the ion are also important, there is an increased probability of electron ejection in the backward direction. The relative influence of these two dynamical effects, as well as the form of the momentum-space target wave function, determines the final shape of the TDCS, such as the position of dips and peaks [3]. In particular, for geometries in which the scattered electron is fast and the ejected electron relatively slow (asymmetric geometry) the binary collisions produce a peak in the cross section (that is, a maximum in ejected electron emission) near the direction of the momentum-transfer vector $\mathbf{K}=\mathbf{k}_0-\mathbf{k}_a$. Collisions involving significant interaction with the ion result in a peak in the cross section in approximately the $-\mathbf{K}$ direction. The relative magnitude of these so-called binary and recoil peaks depends on the particular kinematical conditions. The recoil structure is attributed specifically to a process in which the projectile electron ionizes the target electron, which then scatters elastically (recoils) from the core. As the recoil structure depends on electron-ion interactions, theories which include only the electron-electron interaction cannot model the recoil peak in the TDCS. Briggs [3] and Berakdar and Briggs [4] also suggested that, in addition to structure arising from the above single and double collision processes, certain structures seen in the TDCS when measured in symmetric geometry arise from Coulomb density-of-state factors and from interference between separate scattering amplitudes.

Generally, for intermediate- to high-energy valence-shell ionization, the binary peak dominates the TDCS, with the recoil peak being considerably smaller. Recently, $(e,2e)$ experiments with impact energies in the range 1–3 keV were performed on inner shells of a number of rare-gas targets [5–8]. There is a scarcity of inner shell $(e,2e)$ experiments as they are difficult and time consuming due to the small

*Author to whom correspondence should be addressed. FAX: 61-7-3875 7656. Electronic address: B.Lohmann@sct.gu.edu.au

cross section for inner-shell ionization compared with valence-shell ionization, and the large background of uncorrelated electrons produced by ionization of outer-lying orbitals. However, the results have revealed a number of interesting features in the cross section for this process. A general feature seen in all the experiments is the presence of a very large recoil peak (in comparison with what is observed for valence-shell ionization under similar kinematical conditions) which becomes the dominant feature when the energy of the slow ejected electron is reduced below the binding energy of the inner-shell orbital.

It has been suggested [6] that the interaction of the ejected electron with the static potential of the core is particularly important for inner-shell ionization, since the ionization process takes place relatively close to the nucleus. Experimental results for argon $2p$ ionization and xenon $4d$ ionization suggest that this interaction is particularly strong for the case where the target electron is ejected with a final kinetic energy which is less than the binding energy.

Clearly, a suitable theoretical description of the inner-shell ionization process should include in some way the multiple-scattering processes which are responsible for the presence of a substantial recoil structure. Bickert and coworkers [5,6] measured TDCS for Ar($2p$), Ar($2s$), and Ne($1s$) ionization in the incident energy range 2–3 keV. The lowest ejected energy used in their measurements was 150 eV for the case of Ar($2p$) ionization (cf. a $2p$ binding energy of approximately 249 eV). More recently, Cavanagh and Lohmann [8] measured TDCS for Ar($2p$) ionization at lower incident energy ($\approx$1 keV) and ejected electron energies of 120 and 50 eV. Generally, the shapes of the measured TDCS were shown to be well described by a distorted-wave Born approximation (DWBA) calculation [6,8]. Avaldi *et al.* [7] measured the TDCS for ionization of the Xe($4d$) inner-shell orbital, under conditions not dissimilar to those employed by Cavanagh and Lohmann for their measurements of argon $2p$ ionization. Avaldi *et al.* used an incident energy of approximately 1 keV and ejected electron energies of 20 and 100 eV the former being less than the $4d$ binding energy of about 69 eV. The momentum transfer in their measurements was, however, considerably smaller than that in the measurements of Cavanagh and Lohmann. Avaldi *et al.* found that there were significant discrepancies between their results and a DWBA calculation. Possible reasons proposed for the failure of the DWBA included inadequate representation of a resonant channel competing with the direct process, spherical averaging of the ion static-exchange potential rather than use of the true nonspherical potential, and neglect of possible post-collision interaction between the ejected electron and Auger electrons subsequently emitted when the core hole is filled.

In this paper we present $(e,2e)$ measurements of ionization of the $3d$ inner shell of krypton. These measurements were motivated by the apparent onset of problems with the DWBA calculations in moving between argon and xenon inner-shell ionization. Additionally, Jakubassa-Amundsen [9] recently investigated the region of validity of the Coulomb-Born approximation (CBA) for $(e,2e)$ reactions, and made the point that additional measurements of inner-shell ionization for targets heavier than argon may be used to bridge the gap between inner-shell ionization of argon, where the CBA is poor, and Cu K-shell ionization, where the CBA appears to work well.

Very few experimental $(e,2e)$ investigations of krypton have been performed, even for valence-shell ionization. Electron momentum spectroscopy studies of the $4p$ and $4s$ orbitals were reported by a number of workers [10–13]. High-energy asymmetric coplanar $(e,2e)$ measurements of $4s$ ionization were reported in Ref. [14], while near-threshold $(e,2e)$ measurements of Kr($4p$) ionization were reported in Ref. [15]. Some pioneering $(e,3e)$ measurements for double ionization of krypton ($4p^{-2}$) have also been published [16]. No $(e,2e)$ measurements for ionization of the inner shells of krypton have appeared in the literature.

The $3d_{3/2}$ and $3d_{5/2}$ orbitals in krypton have binding energies of 95.04 and 93.79 eV, respectively. In the experimental TDCS for $3d$ ionization presented in this paper, the coincidence energy resolution is such that the fine structure is not resolved. Measurements have been performed in coplanar asymmetric geometry at two different ejected electron energies, 72 and 50 eV. The latter energy is approximately 2 eV below the $M_{4,5}$-$N_{2,3}N_{2,3}$ manifold of Auger lines arising from relaxation of the ion after $3d$ ionization.

EXPERIMENT

The coincidence spectrometer used for these measurements has been described elsewhere [17]. An incident electron beam is produced by thermionic emission from a tungsten filament and focused into a beam by an electrostatic electron gun. The incident beam crosses, at right angles, a gas jet, produced by gas effusing from a stainless-steel capillary of inner diameter 0.7 mm. The two electrons produced in the ionization pass through two hemispherical electron energy analyzers, and are detected by channel electron multipliers. Although the electrons are indistinguishable, the convention is to refer to the faster electron as the scattered electron, and the other as the ejected electron. Energy conservation means that

$$E_0 = E_a + E_b + \varepsilon_i , \tag{1}$$

where E_0, E_a, and E_b are the energies of the incident, scattered, and ejected electrons, respectively, and ε_i is the binding energy of the orbital in question. The analyzers are mounted on independent turntables and may be rotated in the scattering plane, the plane formed by the incident electron direction, and the scattered electron direction.

Figure 1 is a schematic diagram of the experimental geometry. In the case of coplanar kinematics, the angle $\phi = 0$. The experiments are performed by fixing the position of the scattered electron energy analyzer and measuring the number of ejected electrons as a function of angle, in time coincidence with the scattered electron. Conventional coincidence timing electronics are employed (see Ref. [17]).

The electron energy analyzers are preceded by five-element retarding lenses which reduce (or increase) the energy of the incoming electrons to the pass energy of the analyzer. The energy resolution of the analyzers in the experiments reported here was approximately 1.6% of the pass energy, the latter being 95 eV. The energy width of the incident electron beam was about 0.5 eV, resulting in an over-

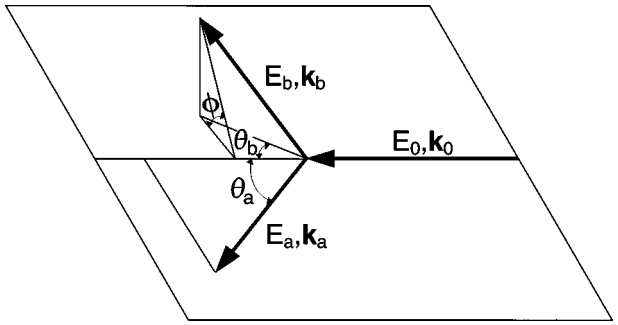

FIG. 1. Schematic diagram of the experimental kinematics. Note that in the coplanar geometry employed here, $\phi = 0$.

all coincidence energy resolution of 2.2 eV. The geometrical angular acceptances of the two analyzers are 0.9° for the scattered electron analyzer and 3.8° for the ejected electron analyzer. The angular resolution of the scattered electron analyzer is kept small in order to better define the scattering angle, and hence the momentum transfer **K**. The angular calibration was determined by measuring the position of the sharp minimum in the cross section for elastic scattering from argon at 100 eV. In the case of the scattered electron analyzer, the zero position was also checked using the symmetry of the double differential cross section.

The scattered electron analyzer was positioned at either $\theta_a = -10°$ or $\theta_a = -15°$ with respect to the incident beam (negative angles are measured anticlockwise with respect to the incident-beam direction, positive angles clockwise). At these forward angles, the analyzer views the whole of the interaction region. The ejected electron analyzer is scanned through a wide angular range (50°–140°), and it is important to check that the whole interaction region is viewed at all angles. This is confirmed by measuring the angular distribution of an Auger line which is known to be isotropic; the resultant distribution is flat to within 5%. TDCS's were measured for $\theta_a = -10°$, $E_b = 50$ eV ($K = 1.59$ a.u.) and $\theta_a = -15°$, $E_b = 72$ eV ($K = 2.31$ a.u.). In both cases the scattered electron energy was set to 880 eV, with the incident energy being determined by Eq. (1). The latter corresponds to the bound Bethe ridge case, where the momentum of the ejected electron $k_b = K$. The binary and recoil regions of each cross section are measured at different times, using the same analyzer to detect the ejected electrons. This is achieved by moving the scattered electron energy analyzer from $-\theta_a$ to $+\theta_a$, while the ejected electron analyzer remains on the same half of the scattering plane. A separate experiment is performed to fix the ratio of the binary to recoil peak. The scattered electron energy analyzer is moved alternately from $-\theta_a$ to $+\theta_a$, while the ejected electron energy analyzer is fixed at a position near the maximum of both the binary and recoil regions. The coincidence count rate is measured for equal times in each region, while the target gas pressure, electron gun current, and other experimental parameters are closely monitored to ensure they remain constant. Although the cross-section measurements are not absolute, the relative normalization of the two cross sections has been experimentally determined. This requires calibrating the transmission efficiency as a function of energy of the ejected electron energy analyzer. This was done by measuring the energy differential cross section for secondary electron production from He, and comparing with the experimental results of Shyn and Sharp [18]. The resulting error of 15% in the normalization between the two cross sections is primarily determined by the stated error in the measurements of Shyn and Sharp; the experimental statistical error in our normalization measurement is considerably smaller than this.

RESULTS AND DISCUSSION

The experimental results have been compared with calculations performed in the DWBA. The calculations were performed by us, using a program code provided by McCarthy [19]. In this formulation, the TDCS is given by

$$\frac{d^5\sigma}{d\Omega_a d\Omega_b dE_a} = (2\pi)^4 \frac{k_a k_b}{k_0} \sum_{av} |\langle \mathbf{k}_a \mathbf{k}_b | T | \alpha \mathbf{k}_0 \rangle|^2, \quad (2)$$

where the subscripts $(0,a,b)$ refer to the incident, scattered (fast) and ejected (slow) electrons, respectively, and α represents the initial bound state. In the DWBA approximation, the T-matrix element is given by

$$\langle \mathbf{k}_a \mathbf{k}_b | T | \alpha \mathbf{k}_0 \rangle = \langle \chi^{(-)}(\mathbf{k}_a) \chi^{(-)}(\mathbf{k}_b) | v_3 | \alpha \chi^{(+)}(\mathbf{k}_0) \rangle. \quad (3)$$

v_3 is the electron-electron Coulomb potential. In the calculations reported here, the distorted wave representing the incident electron is calculated in the atom potential, while the distorted waves representing the outgoing fast and slow electrons are calculated in the ion potential. Exchange is included by using the Furness-McCarthy [20] equivalent local approximation to the exchange potential in the spin-averaged static-exchange potential used as the distorting potential.

Under conditions where the collision is impulsive, the distorted-wave impulse approximation (DWIA) has been successfully applied to valence-shell ionization [21,22], and even with some degree of success to inner-shell ionization [23]. Since one of the cross sections presented here has been measured in bound Bethe ridge kinematics, which corresponds to an impulsive regime, we have also compared the results with a DWIA calculation. In the DWIA the TDCS is given by

$$\frac{d^5\sigma}{d\Omega_a d\Omega_b dE_a} = (2\pi)^4 \frac{k_a k_b}{k_0} f_{ee} N_\alpha \sum_m |M|^2, \quad (4)$$

where

$$|M|^2 = \langle \chi^-(\mathbf{k}_a) \chi^-(\mathbf{k}_b) | \alpha \chi^+(\mathbf{k}_0) \rangle, \quad (5)$$

f_{ee} is the electron-electron collision factor, and N_α is the number of electrons occupying the orbital $|\alpha\rangle$.

The results are presented in Figs. 2 and 3. In Fig. 2, the experimental data were obtained at an incident energy of 1046 eV, a scattered electron energy of 880 eV, an ejected electron energy of 72 eV, and a scattering angle of $-15°$. To obtain the data shown in Fig. 3, the ejected electron energy was lowered to 50 eV (therefore requiring $E_0 = 1024$ eV), and the scattering angle reduced to $-10°$. As the relative magnitude of the two cross sections is fixed by the experimental normalization, the normalization of the data against

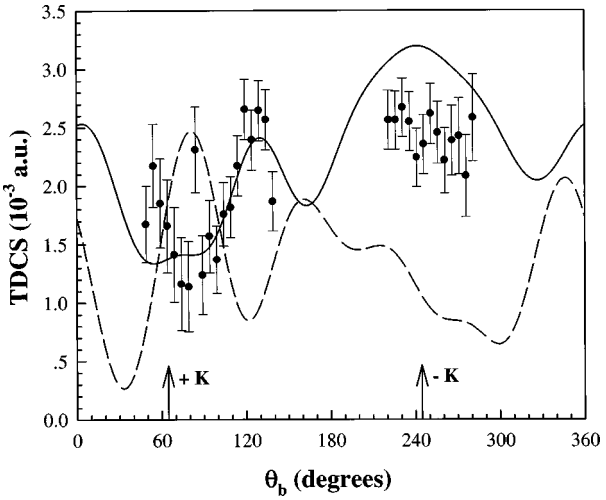

FIG. 2. Triple differential cross section for $3d$ ionization in krypton. Kinematic conditions are $E_0=1046.4$ eV, $E_a=880$ eV, $E_b=72$ eV, and $\theta_a=15°$. The experimental data (●) are relative, and have been normalized (see text) to a distorted-wave Born approximation calculation (solid line). The directions of the momentum transfer, $\mathbf{K}$ and $-\mathbf{K}$, are indicated by arrows. The magnitude of the momentum transfer, $K=2.31$ a.u., corresponds to bound Bethe ridge conditions. The dashed line is a distorted-wave impulse approximation calculation.

the theory is not completely arbitrary, and the two data sets have been normalized to the theory so as to give the best visual fit across both sets.

It is immediately apparent that the experimental results exhibit large recoil structures, indicating a significant interaction between the ejected target electron and the ion. However, although both cross sections correspond to ejected electron energies below the binding energy of the $3d$ orbital, the recoil to binary ratio is only about 1:1 in each case. This is in contrast to the results of Cavanagh and Lohmann [8] for Ar($2p$) ionization, where the recoil peak was almost three times larger than the binary peak for ejected electron energies of 50 and 120 eV. One might postulate that the difference is a target effect, given that in the case of krypton a d orbital is being ionized. However, the results of Avaldi *et al.* [7] for $4d$ ionization in xenon tend to confirm the trend seen in argon $2p$ ionization.

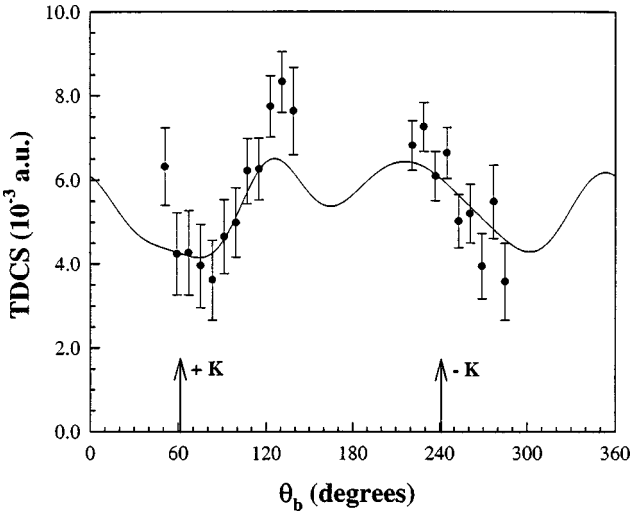

FIG. 3. As for Fig. 2, except that $E_0=1024.4$ eV, $E_b=50$ eV, and $\theta_a=10°$. The solid line is again a distorted-wave Born approximation calculation. The momentum transfer for this case is $K=1.59$ a.u.

The results of the DWBA calculation are shown as the solid line in each graph. The calculation in general does very well in describing the experimental cross section, although there are a few discrepancies such as the binary to recoil ratio in Fig. 2, where the theory overestimates the size of the recoil peak. The experimental cross section also appears to be approaching a maximum near 50° in Fig. 2, while the theoretical cross section is a minimum at this point. The direction of the momentum transfer vector, $+\mathbf{K}$, is shown in the figures, as is $-\mathbf{K}$. Some general observations can be made. In the binary region, the minimum in the measured cross sections occurs at a somewhat larger angle than $+\mathbf{K}$; in the recoil region, for 72-eV ejected energy, the recoil peak has a maximum close to $-\mathbf{K}$, while for 50-eV ejected energy (Fig. 3) the recoil peak occurs at a lower angle than $-\mathbf{K}$; that is, it is moved toward the backward emission direction.

In Fig. 2 we also include a DWIA calculation (dashed line). Somewhat surprisingly, the DWIA is completely inadequate in describing the cross section, predicting maxima where minima are observed, and vice versa (we believe that the agreement between the theory and the experimental point at 84° is fortuitous, with the anomalously high value at this point being purely statistical variation). Zhang, Whelan, and Walters [23] presented DWIA and DWBA calculations for inner-shell ionization of Ar($2s$) and Ar($2p$) in the incident energy range of 2–3 keV, and for Ar($2p$) at 8 keV. Comparison with the available experimental data [5,24] showed that the DWIA did not work well for kinematic conditions far from the bound Bethe ridge, but for kinematics near or on the bound Bethe ridge the DWIA gave good agreement in shape with the data. Zhang, Whelan, and Walters [23] suggested that given the generally good shape agreement of the two calculations for bound Bethe ridge kinematics, absolute measurements were necessary to discriminate between the two theories, since, for most cases they considered, the predicted magnitudes were quite different. However, our results for krypton show that despite being on the bound Bethe ridge, the DWIA is clearly not working. This may be a result of the lower incident energy at which our measurements were performed, resulting in a breakdown of the factorization approximation. In Ref. [23] it was found that for Ne($1s$) ionization at an incident energy of 2700 eV (binding energy 870 eV) the DWIA did not do a good job, despite being on the bound Bethe ridge. This was attributed to the rather low incident energy compared with the binding energy. We note, however, that the ratio of incident energy to binding energy in our krypton measurements is similar to that in the Ar($2p$) measurements of Bickert *et al.* [5], which were well described by a DWIA calculation [23].

When a core hole is produced in the target, the ion is left in an excited state which has a high probability of subsequently decaying by emission of an Auger electron. For $3d$ ionization of krypton, the process may be represented as

$$e_{\text{incident}}+\text{Kr}\rightarrow\text{Kr}^{+}*(3d^{-1})+e_{\text{scattered}}+e_{\text{ejected}}$$
$$\hookrightarrow\text{Kr}^{2+}+e_{\text{Auger}}.$$

Avaldi *et al.* [7], in their measurements on $4d$ ionization in xenon, postulated that some of the discrepancies between their data and the DWBA calculation were the result of neglecting the influence of Auger electrons emitted after the inner-shell ionization. Post-collision interaction (PCI) between the Auger electrons and the ejected electrons has been shown to result in energy shifts of the Auger lines, and distortions of the line shapes due to interference phenomena [25–28]. Avaldi *et al.* [29] have also presented unambiguous evidence of an angular dependence of the effect of PCI on the Auger line shape when the ejected and Auger electrons have equal energies. There is also some evidence that the presence of the Auger electron can affect the TDCS, at least when the ejected electron energy is low [30]. However, it is not clear whether at higher ejected energies the emission of an Auger electron of the same energy as the ejected electron will affect the angular distribution of the ejected electron. In xenon, there are a number of Auger lines resulting from the $4d$ ionization which lie in the region 15–30 eV, and Avaldi *et al.* [7] performed a measurement of Xe($4d$) ionization at an ejected electron energy of 20 eV. In the case of krypton $3d$ ionization, there is a manifold of Auger lines in the region 51–58 eV, as shown in Fig. 4. Given the ejected electron energy resolution of the current measurements (represented schematically in Fig. 4), there should be considerable likelihood of observing the influence of the Auger electrons on the TDCS, if such effects are measurable. The relatively good agreement between the experimental data and the theory in Fig. 3 suggests that the presence of the Auger electrons does not have a significant effect on the cross section.

CONCLUSIONS

Triple differential cross-section measurements have been made for inner-shell electron-impact ionization in krypton, specifically ionization of the $3d$ orbital. The results confirm previous observations on other noble gases of a large recoil peak in the cross section for ejected electron energies below the binding energy of the orbital in question. However, in the case of krypton, the recoil peak is not as prominent as might be expected from trends observed in argon and xenon. Comparison with a distorted-wave Born approximation shows generally good agreement with the data, with a few discrepancies. For the case where bound Bethe ridge kinematics were employed, the results were also compared with a distorted-wave impulse approximation, and it was observed that the latter calculation is completely inadequate in describing inner-shell ionization in this target.

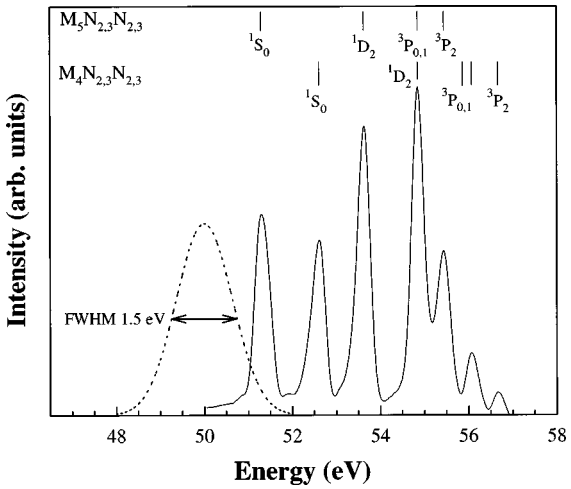

FIG. 4. The Kr $M_{4,5}$-$N_{2,3}N_{2,3}$ Auger lines in the region from 51 to 58 eV, measured in our apparatus in noncoincident mode with an energy resolution of 0.45 eV. The Gaussian profile represents the ejected electron energy resolution during the coincidence measurement, centered at an ejected electron energy of 50 eV.

ACKNOWLEDGMENTS

The authors would like to thank Professor Colm Whelan, Dr. Jens Rasch, and Dr. Stephane Mazevet for helpful discussions and for checking some of the calculated cross sections. The DWBA and DWIA program codes were provided by Professor Ian McCarthy, who also rendered much helpful assistance during the implementation of the codes. This work was supported by the Australian Research Council.

[1] I. E. McCarthy and E. Weigold, Rep. Prog. Phys. **54**, 789 (1991).
[2] A. Lahmam-Bennani, J. Phys. B **24**, 2401 (1991).
[3] J. Briggs, Comments At. Mol. Phys. **23**, 155 (1989).
[4] J. Berakdar and J. S. Briggs, J. Phys. B **27**, 4271 (1994).
[5] P. Bickert, W. Hink, C. Dal Capello, and A. Lahmam-Bennani, J. Phys. B **24**, 4603 (1991).
[6] X. Zhang, C. T. Whelan, H. R. J. Walters, R. J. Allan, P. Bickert, W. Hink, and S. Schönberger, J. Phys. B **25**, 4325 (1992).
[7] L. Avaldi, R. Camilloni, R. Multari, G. Stefani, X. Zhang, H. R. J. Walters, and C. T. Whelan, Phys. Rev. A **48**, 1195 (1993).
[8] S. J. Cavanagh and B. Lohmann, J. Phys. B **30**, L231 (1997).
[9] D. H. Jakubassa-Amundsen, Phys. Rev. A **53**, 2359 (1996).
[10] E. Weigold, S. T. Hood, and I. E. McCarthy, Phys. Rev. A **11**, 566 (1975).
[11] I. Fuss, R. Glass, I. E. McCarthy, A. Minchinton, and E. Weigold, J. Phys. B **14**, 3277 (1981).
[12] K. T. Leung and C. E. Brion, Chem. Phys. **82**, 87 (1983).
[13] R. Nicholson, S. W. Braidwood, I. E. McCarthy, E. Weigold, and M. J. Brunger, Phys. Rev. A **53**, 4205 (1996).
[14] A. Lahmam-Bennani, A. Duguet, and C. D. Dal Capello, J. Electron Spectrosc. Relat. Phenom. **40**, 141 (1986).
[15] P. Selles, J. Mazeau, and A. Huetz, J. Phys. B **23**, 2613 (1990).
[16] A. Lahmam-Bennani, A. Duguet, A. M. Grisogono, and M. Lecas, J. Phys. B **25**, 2873 (1992).

[17] B. Lohmann, X.-K. Meng, and M. Keane, J. Phys. B **25**, 5223 (1992).
[18] T. W. Shyn and W. E. Sharp, Phys. Rev. A **19**, 557 (1979).
[19] I. E. McCarthy, Aust. J. Phys. **48**, 1 (1995).
[20] J. B. Furness and I. E. McCarthy, J. Phys. B **6**, 2280 (1973).
[21] D. H. Madison, I. E. McCarthy, and X. Zhang, J. Phys. B **22**, 2041 (1989).
[22] I. E. McCarthy, Z. Phys. D **23**, 287 (1992).
[23] X. Zhang, C. T. Whelan, and H. R. J. Walters, in (*e*,*2e*) *and Related Processes*, edited by C. T. Whelan, H. R. J. Walters, A. Lahmam-Bennani, and H. Ehrhardt (Kluwer, Dordrecht, 1993), p. 409.
[24] A. Lahmam-Bennani, H. F. Wellenstein, A. Duguet, and A. Daoud, Phys. Rev. A **30**, 1511 (1984).
[25] E. C. Sewell and A. Crowe, J. Phys. B **17**, L547 (1984).
[26] W. Sandner and M. Völkel, J. Phys. B **17**, L597 (1984).
[27] B. Lohmann, J. Phys. B **24**, L249 (1991).
[28] D. K. Waterhouse and J. F. Williams, J. Phys. B **30**, 2845 (1997).
[29] L. Avaldi, P. Belotti, R. Bolognesi, R. Camilloni, and G. Stefani, Phys. Rev. Lett. **75**, 1915 (1995).
[30] G. Stefani, L. Avaldi, A. Lahmam-Bennani, and A. Duguet, J. Phys. B **19**, 3787 (1986).